AGU PUBLICATIONS

Geophysical Research Letters

RESEARCH LETTER
10.1002/2014GL061199

Key Points:
- We newly detected ~3000 low-magnitude foreshocks of the L'Aquila earthquake
- Mid-February migration preceded the April main shock
- A low *b*-value local patch controlled the preparatory stage of the main shock

Correspondence to:
M. Sugan,
msugan@inogs.it

Citation:
Sugan, M., A. Kato, H. Miyake, S. Nakagawa, and A. Vuan (2014), The preparatory phase of the 2009 M_w 6.3 L'Aquila earthquake by improving the detection capability of low-magnitude foreshocks, *Geophys. Res. Lett.*, *41*, doi:10.1002/2014GL061199.

Received 14 JUL 2014
Accepted 18 AUG 2014
Accepted article online 25 AUG 2014

The preparatory phase of the 2009 M_w 6.3 L'Aquila earthquake by improving the detection capability of low-magnitude foreshocks

Monica Sugan[1], Aitaro Kato[2,3], Hiroe Miyake[3], Shigeki Nakagawa[3], and Alessandro Vuan[4]

[1]OGS, Istituto Nazionale di Oceanografia e di Geofisica Sperimentale, Centro Ricerche Sismologiche, Udine, Italy, [2]Earthquake and Volcano Research Center, Graduate School of Environmental Studies, Nagoya University, Nagoya, Japan, [3]Earthquake Research Institute, University of Tokyo, Tokyo, Japan, [4]OGS, Istituto Nazionale di Oceanografia e di Geofisica Sperimentale, Centro Ricerche Sismologiche, Trieste, Italy

Abstract We explored the detection capability of low-magnitude earthquakes before the 6 April 2009 M_w 6.3 L'Aquila event by using a matched filter technique and 512 foreshocks as templates. We analyzed continuous waveforms from 10 broadband seismic stations in a 60 km radius from the epicenter and for ~3 months before the main shock. More than 3000 new events, mostly located on the main shock fault, were detected to define the spatial-temporal evolution of micro-seismicity. The foreshock sequence was active northwest of the M_w 6.3 hypocenter in January, then migrated toward it at a speed of ~0.5 km/day in middle of February. At that time, in a ~4 km^2 patch close to the main shock nucleation point, the cumulative number of earthquakes gradually increased until the M_w 6.3 event. This patch, characterized by a low *b*-value, played a key role in controlling the preparation stage to the 2009 L'Aquila main rupture.

1. Introduction

The 2009 L'Aquila complex foreshock sequence lasted several months affecting not only the main fault plane, but also a system of contiguous fault segments. Double-difference high-resolution relocation of foreshocks [*Chiaraluce et al*., 2011] showed that few events were found in sub-areas that released the most of the coseismic slip and seismicity concentrated in a limited downdip portion of the main fault plane. Previous studies indicated that the foreshock pattern and the main shock rupture process might be controlled by crustal heterogeneities [e.g., *Di Stefano et al*., 2011], infiltration of fluids into the upper crust [*Di Luccio et al*., 2010; *Lucente et al*., 2010; *Terakawa et al*., 2010], and stress changes illuminated by *b*-value mapping [*De Gori et al*., 2012].

The relocated foreshocks mostly activated the deepest northern portion of the L'Aquila main fault plane in the 3 months preceding the M_w 6.3 event. At the end of March 2009, the *M* 3.9 foreshock triggered the seismicity migration along a minor north-south trending structure almost antithetic to the main fault. On 5 April, a few hours before the occurrence of the 01:32 (UTC) main shock, seismicity activated the L'Aquila main fault plane [*Chiaraluce et al*., 2011].

The L'Aquila foreshocks were previously detected by using the short time average (STA) and long time average (LTA) trigger-based methods [e.g., *Allen*, 1978]. To improve the detection capability of the foreshock catalogue, we explored continuous waveforms from permanent seismic stations of the Italian seismic network by using a cross-correlation matched filter technique (MFT) based on the detection of events that strongly resemble templates [e.g., *Kato et al*., 2012]. By increasing the number of detections, we succeeded in lowering the completeness magnitude (M_c) and in collecting further details in order to characterize the spatial and temporal evolution of foreshock seismicity. The main objective was to verify if the new catalogue determined by applying this technique contributes to improving our understanding of the physical processes at the base of the foreshock seismic sequence that evolved in the 2009 L'Aquila main shock.

2. Data and Methods

Seismic events are typically detected by using the STA/LTA methods; they are computationally fast, but their performance is conditioned by the signal-to-noise ratio. The cross correlation of a waveform template with

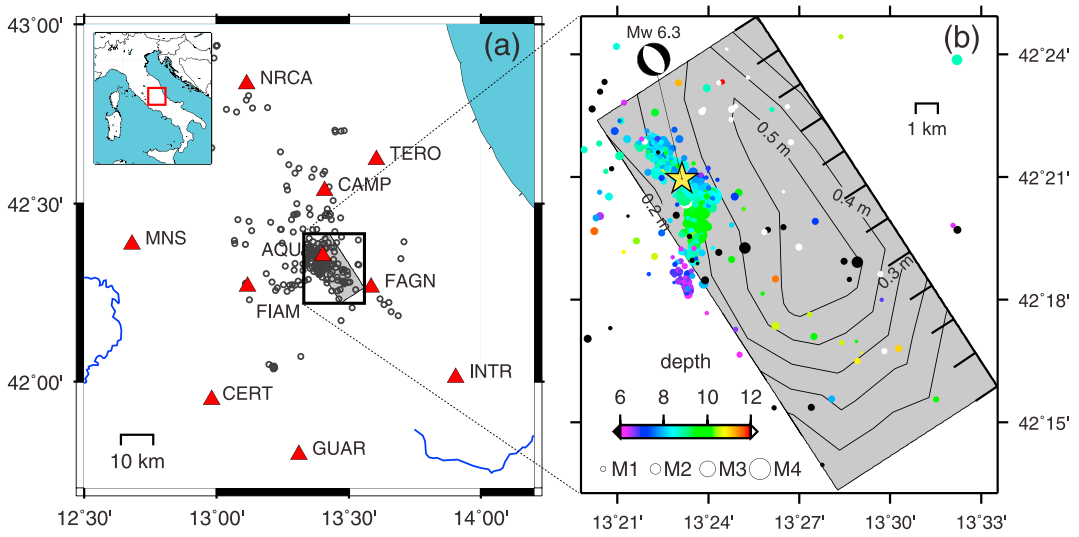

Figure 1. (a) Layout of the L'Aquila region showing the location of permanent Istituto Nazionale di Geofisica e Vulcanologia (INGV) seismic stations (red triangles) used and 512 template events (black circles) selected from the catalogue of *Chiaraluce et al.* [2011]. (b) Zoom view of the location of 419 template events close to the main fault plane with the slip inverted by *Poiata et al.* [2012] using teleseismic data for the 6 April 2009 M_w 6.3 L'Aquila earthquake. Size and color of the template events are drawn as a function of magnitude and hypocentral depth, respectively.

continuously incoming data in a potentially noisy time series represents a powerful method that can increase significantly the detection capabilities with respect to the standard STA/LTA. These methods have recently shown the possibility of significant improvements in many seismological applications such as detection of low-magnitude seismic events [e.g., *Gibbons and Ringdal*, 2006], relocation [e.g., *Schaff and Waldhauser*, 2005], and clustering [e.g., *Harris and Dodge*, 2011].

To recover the missing events over 96 days between 1 January and 6 April 2009, we applied the MFT [e.g., *Kato et al.*, 2012, 2013] to the continuous three-component velocity seismograms recorded at 10 seismic stations around L'Aquila (Figure 1) operated by the Istituto Nazionale di Geofisica e Vulcanologia (INGV). We selected a total of 512 earthquakes between 1 January and 6 April 2009 as template events from the catalogue provided by *Chiaraluce et al.* [2011], relocated using a double-difference algorithm [*Waldhauser and Ellsworth*, 2000].

For each template, we cropped 5 s off the three-component waveforms, starting from 2.5 s before the *S* wave arrival, as computed using a one-dimensional velocity model (Central Italian Apennines—CIA—model) proposed by *Herrmann et al.* [2011]. A two-way 2–5 Hz Butterworth filter was applied to 20 Hz sampled waveforms. The correlation coefficient was calculated between the template event waveforms and target waveforms at each sample. The hypocentral location, the time associated to the origin time, and the magnitude of the new detected events were calculated as described in *Kato et al.* [2013]. A positive detection was set at nine times the median absolute deviation of the mean correlation coefficients for every event and every day. Visual inspection was performed for each new detection before considering it as a positive event. At the end of the procedure, the MFT identified 3571 foreshocks, approximately six times the number in the catalogue of *Chiaraluce et al.* [2011] for the same period.

3. Spatial-Temporal Foreshock Pattern

By applying the MFT to continuous data using the 512 template events, we detected 3571 earthquakes in the magnitude range from −0.4 to 3.9 including templates. Figure 2 demonstrates two examples of new detections by using the MFT.

In Figure 3a we show the comparison between templates and new detected events in terms of number of events per day and magnitude distribution. The MFT increased considerably the detections, with a resultant reduction of the M_c from 1.1 [*Chiaraluce et al.*, 2011] to about 0.5 ± 0.05. On the basis of the

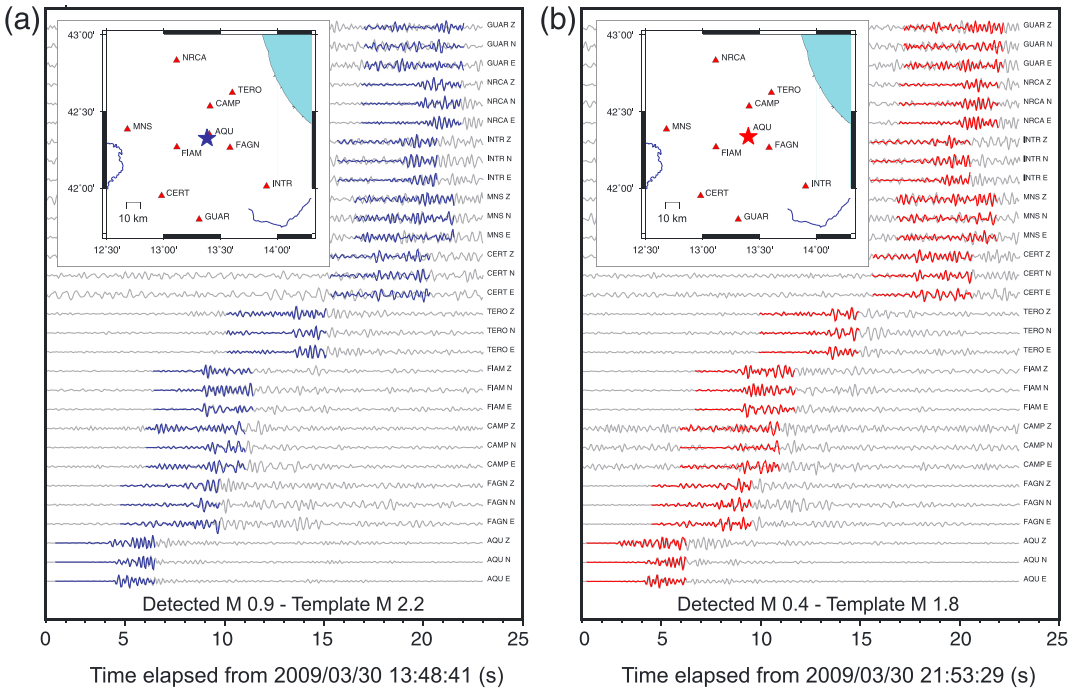

Figure 2. Example of two new detected events. Continuous waveforms on 30 March 2009. Data from 10 three components INGV seismic stations are shown in grey, and template events are colored in (a) blue and (b) red. The station name and component are given on the right of each channel. Each waveform is band-pass filtered between 2 and 5 Hz; the amplitudes of the template events are scaled to balance the continuous waveform. The inset shows the location of seismic stations (red triangles) and the epicenters (stars) of the template events.

seismicity rate changes, we were able to identify nine distinct time windows (TW) within the main shock preparatory phase with different spatial-temporal characteristics. The spatial distribution does not change with respect to *Chiaraluce et al*. [2011], but the space-time evolution is improved to be conspicuous and provides further constraints of the foreshock evolution. The spatial-temporal evolution of the detected seismicity along a cross section oriented at 147° passing throughout the M_w 6.3 event is shown in Figure 3b. During the period from TW1 to TW5, seismicity was mainly confined north-westward of the main shock hypocenter, and the release of seismic energy was modulated in distinct seismic bursts. In mid-February (within TW5), most of the seismicity migrated toward the main shock nucleation point at a speed of about 0.5 km/day, where it persisted from TW6 to TW9. In Figure 3c we discriminate new detections with respect to templates to clarify their impact in the definition of the migration pattern within TW5. Starting and end of migration within TW5 are defined following the spatial-temporal distribution of the events.

TW7 showed a clear reduction in seismicity from 3 to 10 March, until 11 March, when an M 3.2 event triggered a swarm close to the main shock hypocenter. TW8 showed again a reduction in seismicity at the beginning of the time window and a following increase in the number of earthquakes culminating with the event in TW9 occurring on 30 March at 13:38 UTC (M 3.9). Excluding this event, TW9 was characterized by other six events with $M > 3$, all reported in *Chiaraluce et al*. [2011].

The spatial variation of the seismicity pattern, within the different time windows, is shown in Figure 4. Southward migration of foreshocks was observed during the mid-February (TW5). Most of the earthquakes were located within the main shock fault plane along the northwest to southeast strike from TW1 to TW5 with a subsequent change in the alignment from north to south during the week before the main shock (TW9). In the TW9 phase, an area located south of the M_w 6.3 hypocenter was activated (Panel 9 in Figure 4). As previously observed [*Chiaraluce et al*., 2011; *Valoroso et al*., 2013], a swarm of shallower events was found on an antithetic plane facing the main fault.

For the new foreshock catalogue, spatial variations of the *b*-value were calculated using the ZMAP code [*Wiemer*, 2001] (Figure 5a). We used nodes spaced at 0.002° with at least 50 events above M_c within a radius of

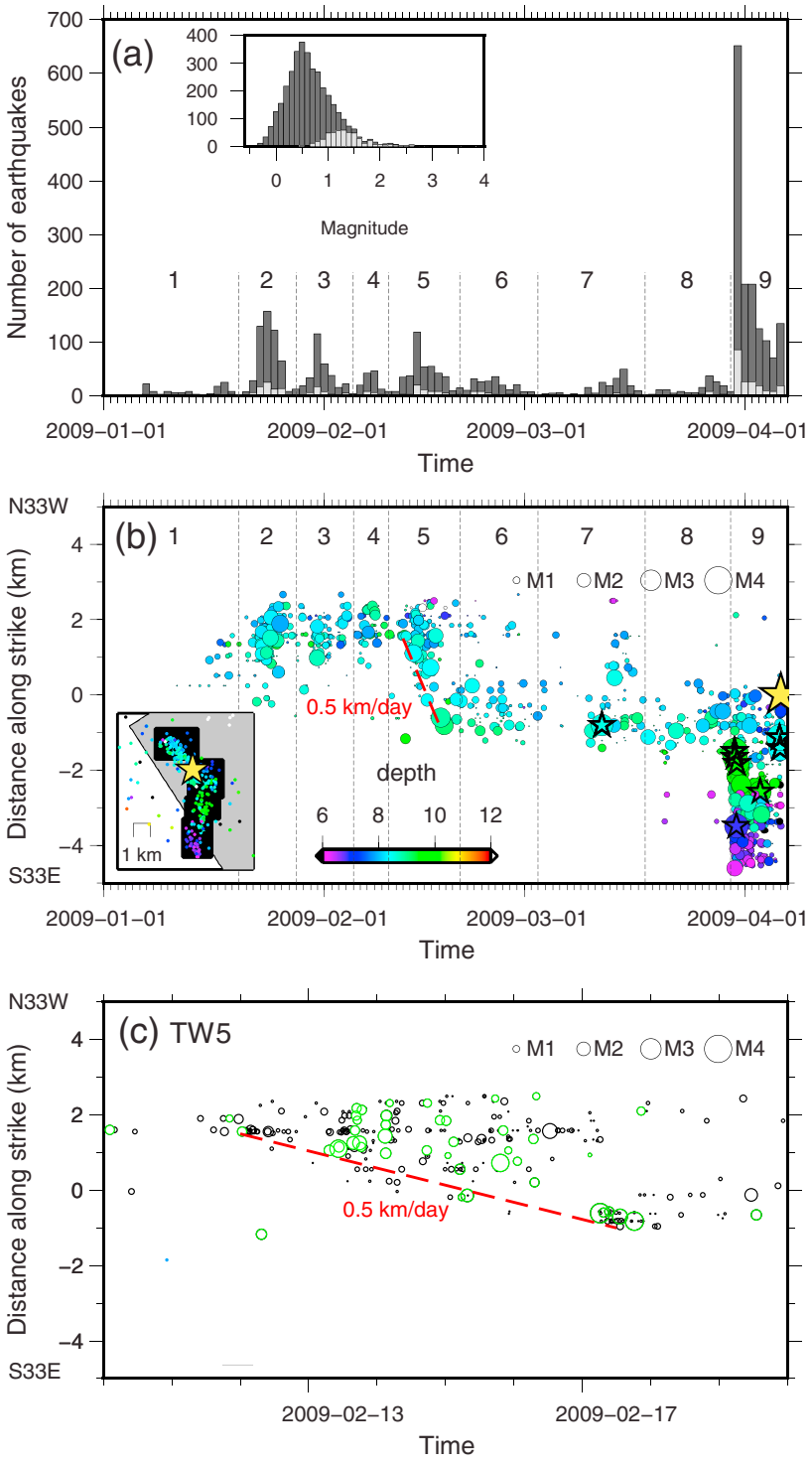

Figure 3. (a) Histogram showing the number of earthquakes per day (using center bin) and per magnitude (0.1 bin) for the templates (light grey) and for the events detected by the matched filter technique (MFT) (black grey). Numbers from 1 to 9 mark different time windows (TW) of the L'Aquila seismic sequence in the period from 1 January to 6 April 2009. (b) Space-time diagram of the detected events for the black area shown in the inset. The tiny seismicity observed at the beginning of January 2009 in Figure 3a is located outside this area. Distance taken along a 147° oriented cross section; 0 distance corresponds to hypocenter of the L'Aquila main shock, positive distance represents the seismicity in the northern sector, negative distance represents the seismicity in the southern sector. The L'Aquila main shock (yellow star), earthquakes with $M > 3.0$ (simple stars), and the migration of earthquakes starting from 12 February (red dashed line) are shown. (c) Space-time diagram of the detected events for TW5; green and black circles correspond to template events [*Chiaraluce et al.*, 2011] and new detections, respectively.

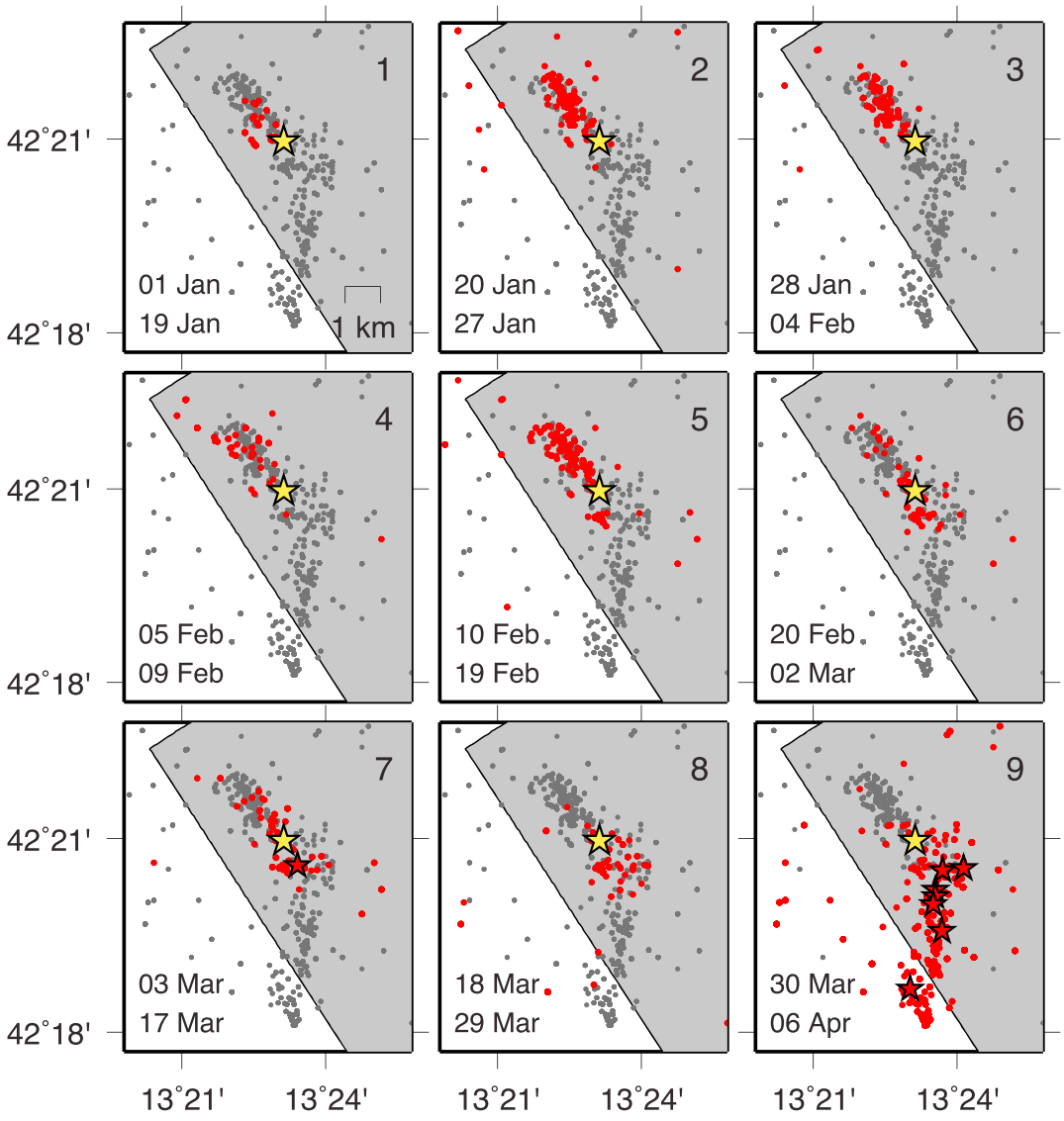

Figure 4. Spatial-temporal evolution of the detected seismicity around the epicentral area in the period from 1 January to 6 April for the nine different time windows shown in Figure 3. Grey dots: MFT detected earthquake; red dots: MFT detected earthquake in the corresponding time window; yellow star: L'Aquila main shock; red star: events with $M > 3.0$; grey area: area of coseismic slip due to the main shock, as shown in Figure 1.

0.8 km. Values and uncertainties were computed using the maximum curvature algorithm by bootstrapping each sample with 100 realizations. The analysis is shown in Figure 5a, where we identified four sub-areas (S1, S2, S3, and S4) from north to south with different average *b*-values.

For each sub-area, we plot the depth section of hypocenters perpendicular to the fault strike (Figure 5b), the M_c and the associated *b*-value (Figure 5c), and the cumulative number of events above the M_c (Figure 5d). We used the same M_c value of 0.47 for S1, S2, and S3. We discovered that S2 has a low *b*-value of 0.79 close to the main shock hypocenter, bounded by two sub-areas (S1 and S3) of normal *b*-values of around 1 located both north and south of it. S4 area, which encloses shallower seismicity located off the main fault plane, as previously described, is characterized by a high *b*-value such as 1.26. In Figure 5d, it can be observed that the cumulative number of earthquake for S2 with low *b*-value patch continuously increased, with different rate, from the mid-February to 6 April. In particular, the significant increase in seismicity during TW9, after the foreshocks on 30 March and 5 April, is coupled with an increase of the activated area/volume (Panel 9 in Figure 4).

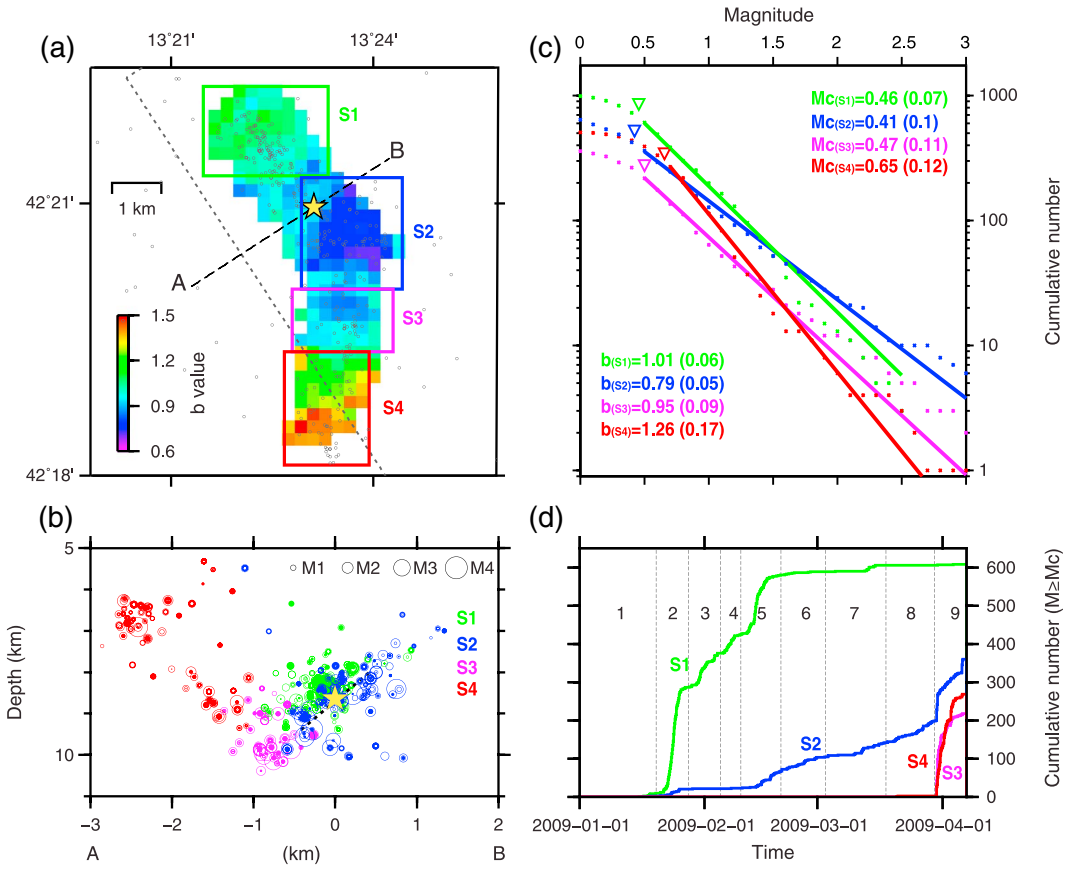

Figure 5. (a) *b*-value map calculated using the ZMAP code [*Wiemer*, 2001]. (b) Spatial event distribution along the A–B vertical cross section for each sub-area (S1–S4). (c) Completeness magnitude (M_c) and associated *b*-value for each sub-area. (d) Cumulative number of events above the M_c for each sub-area (see text for details).

4. Discussion and Conclusions

The preparatory seismic sequence before the M_w 6.3 L'Aquila earthquake of 6 April 2009 was characterized by three different phases, each one with distinct peculiarities (Figure 5): seismic bursts with a normal *b*-value in the northwest of the main shock hypocenter until the mid-February (S1), the gradual increase in seismicity with low *b*-value adjacent to the main shock hypocenter from mid-February to the main shock initiation (S2), and the most intensive phase with moderate to high *b*-values in the south of the main shock hypocenter during a week before the main shock (from March 30 to April 6) (S3 and S4).

The low *b*-value patch (S2) is adjacent to the main shock nucleation and along the downdip edge of the largest slip area of the main shock rupture (Figure 5). *De Gori et al.* [2012] reported that low-*b*-value was observed near the main shock hypocenter using the existing catalogue. Our newly detected foreshock catalog improved the spatial resolution of the *b*-value map. An area of low *b*-value patch (S2) of about 4 km^2 (Figure 5a), localized southeast of the main shock, is quantitatively defined. It has been well recognized that low *b*-value patches are located near initiation points of main shock ruptures prior to some earthquakes as the 2004 M_w 9.1 Sumatra, 2011 M_w 9.0 Tohoku-Oki, and 2004 M_w 6.0 Parkfield earthquakes [*Schorlemmer et al.*, 2005; *Nanjo et al.*, 2012]. On the basis of laboratory fracture experiments of rocks [e.g., *Mogi*, 1968; *Lei et al.*, 2003], low *b*-value reflects increasing stress due to fracture growth on a ruptured area, particularly on its boundaries. We thus interpret that the local low *b*-value patch very close to the main shock hypocenter might be a highly stressed patch of the fault before the main shock rupture.

The final phase with the most intensive seismicity could be linked to diffusion of highly pressurized fluids into the hanging wall volume [e.g., *Lucente et al.*, 2010; *Terakawa et al.*, 2010]. According to *Lucente et al.* [2010], strong changes in the V_p/V_s ratio were monitored after 30 March 2009, mainly in the hanging wall, and could be

interpreted as the dilatancy-diffusion transfer processes of fluids into the hanging wall. The seismicity related to the fluid diffusion was located on the shallow antithetic plane facing the main shock fault (S4 in Figure 5). The *b*-value of the antithetic plane seismicity was higher than 1.2, supporting the involvements of crustal fluids [e.g., *Wiemer and Benoit*, 1996]. These *b*-value anomalies suggest that seismic behavior is strongly controlled by stress heterogeneities and material properties of the upper crust.

The cumulative number of earthquakes in the low *b*-value patch (S2) continuously increased from mid-February to the main shock initiation. This seismic behavior suggests that a tectonic loading process (e.g., a slow-slip transient) might be dominant rather than nearby triggering as in epidemic-type cascade sequences [e.g., *Mignan*, 2012; *Marsan et al*., 2013]. In addition, the earthquake migration at a speed of ~0.5 km/day toward the initiation point of the main shock rupture supports a possible slow-slip transient acting during mid-February. The slow-slip transient could have caused the stress loading on the main shock nucleation point, possibly contributing to the low *b*-value anomaly (S2). Earthquake migrations indicating slow-slip transients were similarly observed prior to subduction zone earthquakes such as the 2011 M_w 9.0 Tohoku-Oki and 2014 M_w 8.1 Iquique earthquakes [e.g., *Kato et al*., 2012; *Bouchon et al*., 2013; *Brodsky and Lay*, 2014; *Kato and Nakagawa*, 2014; *Ruiz et al*., 2014]. It is noteworthy that the migrating speed and distance scale before the L'Aquila main shock are lower and smaller than those of subduction zone earthquakes. Given these considerations, the local patch near the main shock nucleation, which is characterized by low *b*-value, migrating seismicity, and gradual increase in cumulative earthquakes, might have played a key role in the preparatory stage of the 6 April 2009 M_w 6.3 L'Aquila earthquake.

Acknowledgments

We acknowledge Andrew Newman and two anonymous reviewers for insightful comments. We are grateful to Istituto Nazionale di Geofisica e Vulcanologia (INGV) for making available seismic data from national permanent stations and to Lauro Chiaraluce and co-authors for providing the parametric catalogue of foreshocks [*Chiaraluce et al*., 2011]. The data to support this article are available from INGV accessing the European Integrated Data Archive (http://eida.rm.ingv.it/). This study is funded by a joint research project within the executive program of scientific and technological cooperation between Italy and Japan for the period 2013–2015. We thank Y. Haryu for support in converting the waveform data. Figures were produced using the Generic Mapping Tools version 5.0 (www.soest.hawaii.edu/gmt; *Wessel and Smith* [1991]).

The Editor thanks Kevin Chao and an anonymous reviewer for assistance in evaluating this manuscript.

References

Allen, R. (1978), Automatic earthquake recognition and timing from single traces, *Bull. Seismol. Soc. Am.*, *68*, 1521–1532.

Bouchon, M., V. Durand, D. Marsan, H. Karabulut, and J. Schmittbuhl (2013), The long precursory phase of most large interplate earthquakes, *Nat. Geosci.*, *6*, 299–302, doi:10.1038/ngeo1770.

Brodsky, E., and T. Lay (2014), Recognizing foreshocks from the 1 April 2014 Chile earthquake, *Science*, *344*, 700–702, doi:10.1126/science.1255202.

Chiaraluce, L., L. Valoroso, D. Piccinini, R. Di Stefano, and P. De Gori (2011), The anatomy of the 2009 L'Aquila normal fault system (central Italy) imaged by high resolution foreshock and aftershock locations, *J. Geophys. Res.*, *116*, B12311, doi:10.1029/2011JB008352.

De Gori, P., F. P. Lucente, A. M. Lombardi, C. Chiarabba, and C. Montuori (2012), Heterogeneities along the 2009 L'Aquila normal fault inferred by the b-value distribution, *Geophys. Res. Lett.*, *39*, L15304, doi:10.1029/2012GL052822.

Di Luccio, F., G. Ventura, R. Di Giovambattista, A. Piscini, and F. R. Cinti (2010), Normal faults and thrusts reactivated by deep fluids: The 6 April 2009 Mw 6.3 L'Aquila earthquake, central Italy, *J. Geophys. Res.*, *115*, B06315, doi:10.1029/2009JB007190.

Di Stefano, R., C. Chiarabba, L. Chiaraluce, M. Cocco, P. De Gori, D. Piccinini, and L. Valoroso (2011), Fault zone properties affecting the rupture evolution of the 2009 Mw 6.1 L'Aquila earthquake (central Italy): Insights from seismic tomography, *Geophys. Res. Lett.*, *38*, L10310, doi:10.1029/2011GL047365.

Gibbons, S. J., and F. Ringdal (2006), The detection of low magnitude seismic events using array-based waveform correlation, *Geophys. J. Int.*, *165*, 149–166.

Harris, D. B., and D. A. Dodge (2011), An autonomous system of grouping events in a developing aftershock sequence, *Bull. Seismol. Soc. Am.*, *101*, 763–774.

Herrmann, R. B., L. Malagnini, and I. Munafò (2011), Regional moment tensors of the 2009 L'Aquila earthquake sequence, *Bull. Seismol. Soc. Am.*, *101*, 975–993.

Kato, A., and S. Nakagawa (2014), Multiple slow-slip events during a foreshock sequence of the 2014 Iquique, Chile Mw 8.1 earthquake, *Geophys. Res. Lett.*, *41*, 5420–5427, doi:10.1002/2014GL061138.

Kato, A., K. Obara, T. Igarashi, H. Tsuruoka, S. Nakagawa, and N. Hirata (2012), Propagation of slow slip leading up to the 2011 Mw 9.0 Tohoku-Oki earthquake, *Science*, *335*, 705–708, doi:10.1126/science.1215141.

Kato, A., J. Fukuda, and K. Obara (2013), Response of seismicity to static and dynamic stress changes induced by the 2011 M9.0 Tohoku-Oki earthquake, *Geophys. Res. Lett.*, *40*, 3572–3578, doi:10.1002/grl.50699.

Lei, X.-L., K. Kusunose, T. Satoh, and O. Nishizawa (2003), The hierachical rupture process of a fault: An experimental study, *Phys. Earth Planet. Inter.*, *137*, 213–228.

Lucente, F. P., P. De Gori, L. Margheriti, D. Piccinini, M. Di Bona, C. Chiarabba, and N. Piana Agostinetti (2010), Temporal variation of seismic velocity and anisotropy before the 2009 Mw 6.3 L'Aquila earthquake, Italy, *Geology*, *38*, 1015–1018, doi:10.1130/G31463.1.

Marsan, D., E. Prono, and A. Helmstetter (2013), Monitoring aseismic forcing in fault zones using earthquake time series, *Bull. Seismol. Soc. Am.*, *103*, 169–179, doi:10.1785/0120110304.

Mignan, A. (2012), Seismicity precursors to large earthquakes unified in a stress accumulation framework, *Geophys. Res. Lett.*, *39*, L21308, doi:10.1029/2012GL053946.

Mogi, K. (1968), Source locations of elastic shocks in the fracturing process in rocks, *Bull. Earthquake Res. Inst., Univ. Tokyo*, *46*, 1103–1125.

Nanjo, K. Z., N. Hirata, K. Obara, and K. Kasahara (2012), Decade-scale decrease in b value prior to the M9-class 2011 Tohoku and 2004 Sumatra quakes, *Geophys. Res. Lett.*, *39*, L20304, doi:10.1029/2012GL052997.

Poiata, N., K. Koketsu, A. Vuan, and H. Miyake (2012), Low-frequency and broad-band source models for the 2009 L'Aquila, Italy, earthquake, *Geophys. J. Int.*, *191*, 224–242, doi:10.1111/j.1365-246X.2012.05602.x.

Ruiz, S., M. Metois, A. Fuenzalida, J. Ruiz, F. Leyton, R. Grandin, C. Vigny, R. Madariaga, and J. Campos (2014), Intense foreshocks and a slow slip event preceded the 2014 Iquique M_w 8.1 earthquake, *Science*, *345*, 1165–1169, doi:10.1126/science.1256074.

Schaff, D. P., and F. Waldhauser (2005), Waveform cross correlation based differential travel-time measurements at the northern California Seismic Network, *Bull. Seismol. Soc. Am.*, *95*, 2446–2461, doi:10.1785/0120040221.

Schorlemmer, D., S. Wiemer, and M. Wyss (2005), Variations in earthquake-size distribution across different stress regimes, *Nature*, *437*, 539–542, doi:10.1038/nature04094.

Terakawa, T., A. Zoporowski, B. Galvan, and S. A. Miller (2010), High-pressure fluid at hypocentral depths in the L'Aquila region inferred from earthquake focal mechanisms, *Geology*, *38*, 995–998, doi:10.1130/G31457.1.

Valoroso, L., L. Chiaraluce, D. Piccinini, R. Di Stefano, D. Schaff, and F. Waldhauser (2013), Radiography of a normal fault system by 64,000 high-precision earthquake locations: The 2009 L'Aquila (central Italy) case study, *J. Geophys. Res. Solid Earth*, *118*, 1156–1176, doi:10.1002/jgrb.50130.

Waldhauser, F., and W. L. Ellsworth (2000), A double-difference earthquake location algorithm: Method and application to the northern Hayward Fault, California, *Bull. Seismol. Soc. Am.*, *90*, 1353–1368, doi:10.1785/0120000006.

Wessel, P., and W. Smith (1991), Free software helps map and display data, *Eos Trans. AGU*, *72*, 441–446, doi:10.1029/90EO00319.

Wiemer, S. (2001), A software package to analyze seismicity: ZMAP, *Seismol. Res. Lett.*, *72*, 374–383.

Wiemer, S., and J. P. Benoit (1996), Mapping the b-value anomaly at 100 km depth in the Alaska and New Zealand subduction zones, *Geophys. Res. Lett.*, *23*, 1557–1560, doi:10.1029/96GL01233.